



CHORUS

This is the accepted manuscript made available via CHORUS. The article has been published as:

Tuning of superconductivity by Ni substitution into noncentrosymmetric $\text{ThCo}_{1-x}\text{Ni}_x\text{C}_2$

T. W. Grant, O. V. Cigarroa, P. F. S. Rosa, A. J. S. Machado, and Z. Fisk

Phys. Rev. B **96**, 014507 — Published 10 July 2017

DOI: [10.1103/PhysRevB.96.014507](https://doi.org/10.1103/PhysRevB.96.014507)

Tuning of superconductivity by Ni substitution into noncentrosymmetric $\text{ThCo}_{1-x}\text{Ni}_x\text{C}_2$

T.W. Grant^{1,2}, O.V. Cigarroa², P.F.S. Rosa¹, A.J.S. Machado², and Z. Fisk¹

¹ Department of Physics and Astronomy, University of California-Irvine, Irvine, CA 92697, USA

² Escola de Engenharia de Lorena, Universidade de São Paulo, P.O. Box 116, Lorena, SP, 12602-810, Brazil

ABSTRACT

The recently discovered noncentrosymmetric superconductor ThCoC_2 was observed to show unusual superconducting behavior with a critical temperature of $T_c=2.65\text{K}$. Here we investigate the effect of Nickel substitution on the superconducting state in $\text{ThCo}_{1-x}\text{Ni}_x\text{C}_2$. Magnetization, resistivity, and heat capacity measurements demonstrates Ni substitution has a dramatic effect with critical temperature increased up to $T_c=12.1\text{K}$ for $x=0.4$ Ni concentration, which is a rather high transition temperature for a noncentrosymmetric superconductor. In addition, the unusual superconducting characteristics observed in pure ThCoC_2 appear to be suppressed or tuned with Ni substitution towards a more conventional fully gapped superconductor.

I. INTRODUCTION

Most known superconductors possess an inversion center in their crystal structure and are usually well described by the BCS theory of superconductivity.¹ In this framework, the Cooper pairs that produce the superconducting state can be classified as either even-parity spin singlet, or an odd-parity spin triplet state in accordance to the Pauli exclusion principle and parity conservation.^{2,3} However, if the crystal structure does not have an inversion center (noncentrosymmetric), this removes the parity constraint on the Cooper pair classification and allows for an admixture of spin-singlet and spin-triplet pairing into a mixed-parity pairing state.⁴⁻⁸ In noncentrosymmetric (NCS) superconductors, an asymmetric potential gradient yields an antisymmetric spin-orbit coupling (ASOC), which breaks the spin degeneracy and splits the Fermi surface in two by spin orientation.^{6,7} This

unusual pairing and tunability by the strength of the ASOC can manifest itself in unconventional superconducting behavior, such as a nodal superconducting energy gap, and therefore NCS superconductors are good materials to explore exotic superconducting properties.^{9,10}

Research interest into NCS superconductors expanded significantly after the discovery of unconventional superconductivity in CePt_3Si ,¹¹ along with other heavy fermion (HF) compounds such as UIr , CeRhSi_3 and CeIrSi_3 .¹²⁻¹⁴ However, the coexistence with magnetism and strong electron-correlation in the HF compounds greatly complicates the underlying physics due solely to the NCS crystal structure, as both effects can give rise to unconventional superconductivity. It is therefore highly desirable to explore the superconductivity in weakly correlated NCS systems in order to study the effect of the ASOC on the superconducting state. The superconducting properties of several weakly correlated NCS systems have been extensively investigated, with notable examples such as: $\text{Li}_2(\text{Pd,Pt})_3\text{B}$, Y_2C_3 , $\text{Mg}_{10}\text{Ir}_{19}\text{B}_{16}$, Ru_7B_3 , LaIrP , $\text{Mo}_3\text{Al}_3\text{C}$, and with particular interest for this work LaNiC_2 .¹⁵⁻²⁹

A large series of rare-earth (R) carbides RNiC_2 and RCoC_2 crystallize in the NCS CeNiC_2 prototype structure, which is in the base centered orthorhombic space group $\text{Amm}2$.³⁰ These compounds generally display magnetic order arising from the 4f electrons confined to the rare earth sites,³¹ in addition to the series being near a charge density wave (CDW) instability.³² The nonmagnetic LaNiC_2 becomes superconducting below its critical temperature of $T_c=2.7\text{K}$ and has demonstrated both conventional and unconventional behavior. Early conflicting heat capacity reports concluded both a nodal and fully gapped order parameter, in addition to nuclear quadrupole resonance (NQR) experiments concluding conventional BCS superconductivity.²⁷⁻²⁹ However, more recent experiments have observed unconventional behavior, such as intriguing time reversal symmetry (TRS) breaking in muon-spin relaxation measurements, a nodal energy gap from very-low temperature magnetic penetration depth measurements, and a proposed multi-gap superconductivity due to the moderate value of the ASOC in LaNiC_2 .³³⁻³⁵ The isostructural compound ThCoC_2 was recently discovered to be a new NCS superconductor with a critical temperature of $T_c=2.65\text{K}$.³⁶ The superconductivity of ThCoC_2 was found to exhibit unconventional behavior with a strong positive curvature in the upper critical field H_{c2}

phase diagram, a diminished heat capacity jump and nonexponential temperature dependence in the electronic specific heat. Within this context, this work probes the superconducting state in ThCoC_2 by chemical substitution of elemental Ni into the Co site in the series of compounds $\text{ThCo}_{1-x}\text{Ni}_x\text{C}_2$. The following results of magnetization, resistivity, and heat capacity measurements demonstrate that Ni substitution has a significant effect on the superconducting state of ThCoC_2 .

II. EXPERIMENTAL

Polycrystalline $\text{ThCo}_{(1-x)}\text{Ni}_x\text{C}_2$ samples were synthesized by arc-melting with varying Ni concentration in the range of $0 \leq x \leq 0.7$ and sample mass of 0.4-0.5g. The constituent high purity elements were melted together on a water-cooled Cu hearth in an arc-furnace under UHP Ar atmosphere and using a Zr oxidizing getter. The samples were flipped over and re-melted several times to insure good homogeneity. In order to increase sample quality and insure thermodynamic equilibrium, the samples were sealed in evacuated quartz tubes and annealed at 1100 °C for two weeks. Powder X-ray diffraction (XRD) patterns were obtained in a Rigaku MultiFlex diffractometer using $\text{CuK}\alpha$ radiation. The lattice parameters were determined by using DicVol and Fullprof software and simulation. All refinements were considered final when $C^2 = 2$ and $W_{\text{RP}}=5$ or less. Magnetization measurements were performed down to $T=1.8\text{K}$ using a commercial VSM-SQUID magnetometer by Quantum Design. Electrical resistivity and heat capacity measurements were obtained using a physical property measurement system (PPMS) also by Quantum Design. The samples were polished into flat blocks for best results, with typical size of $\sim 2.5 \text{ mm} \times 1.0 \text{ mm} \times 0.5 \text{ mm}$ for resistivity measurements and typical mass of $\sim 20\text{mg}$ for heat capacity measurements. The heat capacity was measured by field cooled (FC) sweeps with various applied magnetic fields up to 9T in the temperature range of 2K-20K with a ^4He calorimeter using the relaxation method. Resistivity measurements were obtained from 2-300K with applied magnetic field also up to 9T using the standard four-probe method, where fine platinum wires were attached as voltage and current leads using silver epoxy and were measured using a 5mA applied current.

III. RESULTS AND DISCUSSION

First, in order to verify the purity of the samples used for superconducting characterization, XRD patterns were obtained on the annealed Ni substituted samples $\text{ThCo}_{1-x}\text{Ni}_x\text{C}_2$. The samples with nominal Ni concentration up to $x=0.5$ were found to be single phase with all the encountered peaks indexed to the orthorhombic $\text{Amm}2$ space group that is characteristic of the NCS CeNiC_2 prototype structure. Samples with Ni concentration above this limit were not stable and slowly decompose into powder even after annealing. This behavior suggests a substitution limit for Ni close to $x=0.5$, which is surprisingly high considering the compound ThNiC_2 is not known to form. Figure 1 shows the refined cell parameters along with the cell volume across the Ni substitution range. The cell parameter a shows a systematic increase with increasing concentration x , while the b parameter slowly decreases and c remains relatively constant. This results in a small cell distortion with a net expansion of the unit cell volume. The short distance between the CoC_2 sheets are increasing in order to account for the slightly larger Ni atom, while the in-plane b dimension is slowly contracting likely due to the C-C dimer with electron doping from Ni. It is important to note that reliable C-C distances can not be determined from powder XRD. As a stiffening of the bond in the C-C dimer could significantly influence the band structure and superconducting state,³⁷ a future detailed study of the crystal structure by neutron diffraction or single crystal XRD is desirable. An antipressure effect was also seen in LaNiC_2 by Cu substitution in the series $\text{LaNi}_{1-x}\text{Cu}_x\text{C}_2$,³⁸ where they report a small increase in the superconducting critical temperature from 2.7 to 3.4K for Cu concentration up to $x=0.25$. However, Cu substitution is electronically different as it has a full d band, compared to the partially filled $3d^7$ of Co and $3d^8$ of Ni. This difference is observed with Cu substitution only increasing the c cell parameter and quickly approaching its solubility limit for Cu around $x=0.2$. In conjunction with the pure chemical pressure effect by Y substitution $\text{La}_{1-x}\text{Y}_x\text{NiC}_2$ slowly suppressing the critical temperature,³⁹ it appears that an increased cell volume is favorable to the superconducting state in this NCS system.

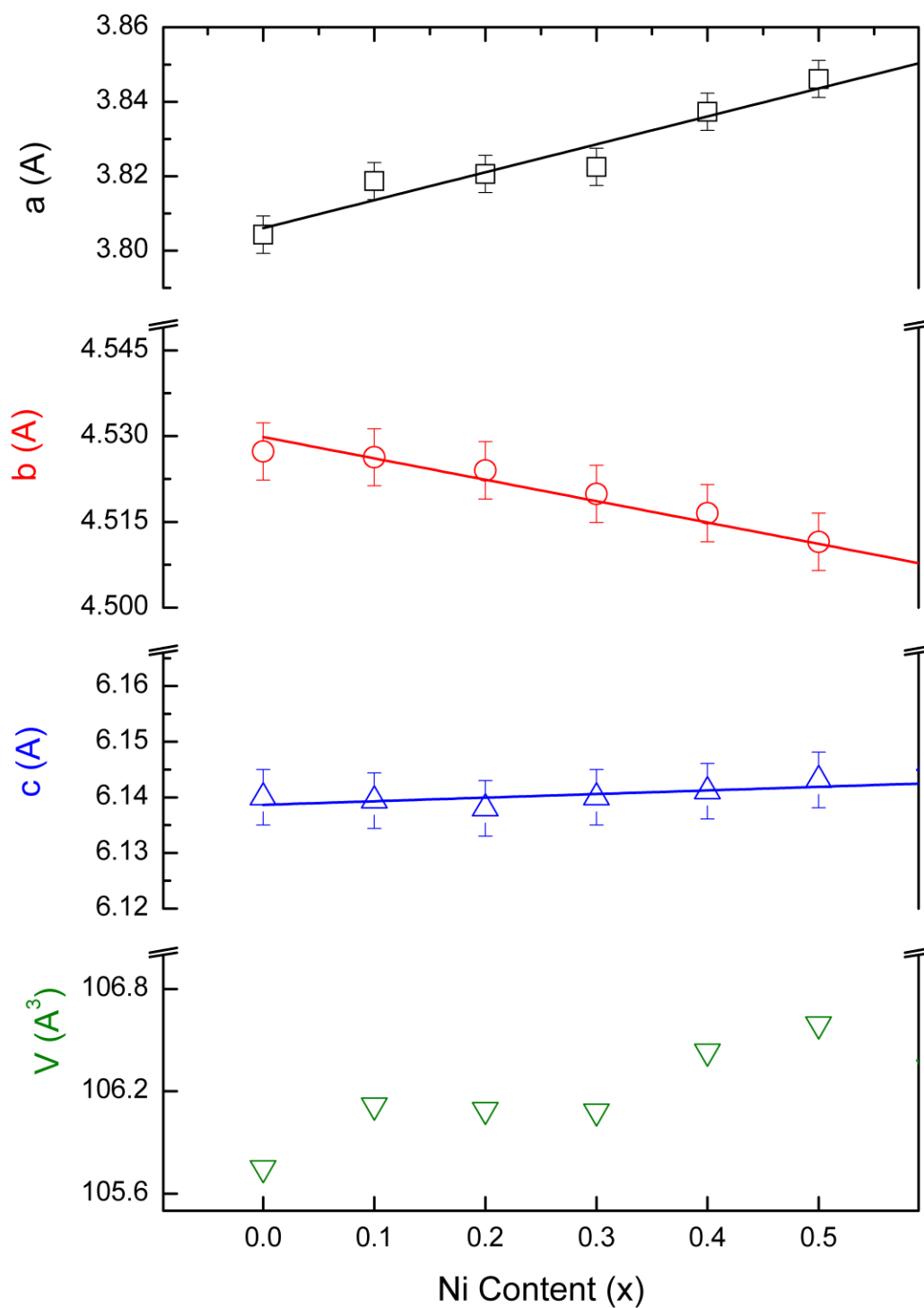


FIG. 1. The refined cell parameters and volume from the XRD patterns with respect to Ni substitution x in the samples $\text{ThCo}_{1-x}\text{Ni}_x\text{C}_2$.

The temperature dependent magnetization results for the annealed $\text{ThCo}_{(1-x)}\text{Ni}_x\text{C}_2$ samples are shown in Fig. 2, where the zero-field cooled (ZFC) and field cooled (FC) sweep method is used with an applied magnetic field of $H=50$ Oe. Large diamagnetic transitions are clearly seen in all the samples during the ZFC sweeps, which is a clear indication of superconductivity. The superconducting transition temperature T_c increases dramatically with Ni concentration and peaks at $x=0.4$ with an onset critical temperature up to $T_c=12\text{K}$, which is rather high for a NCS superconductor and 4.5 times higher than the pure compound ThCoC_2 at 2.65K . The estimated superconducting volume fractions, without correcting for demagnetization or sample size effects, are all nearly 100% with several samples displaying signal saturation at low temperature, which are good indications of bulk superconductivity in the samples and not due to screening effects.

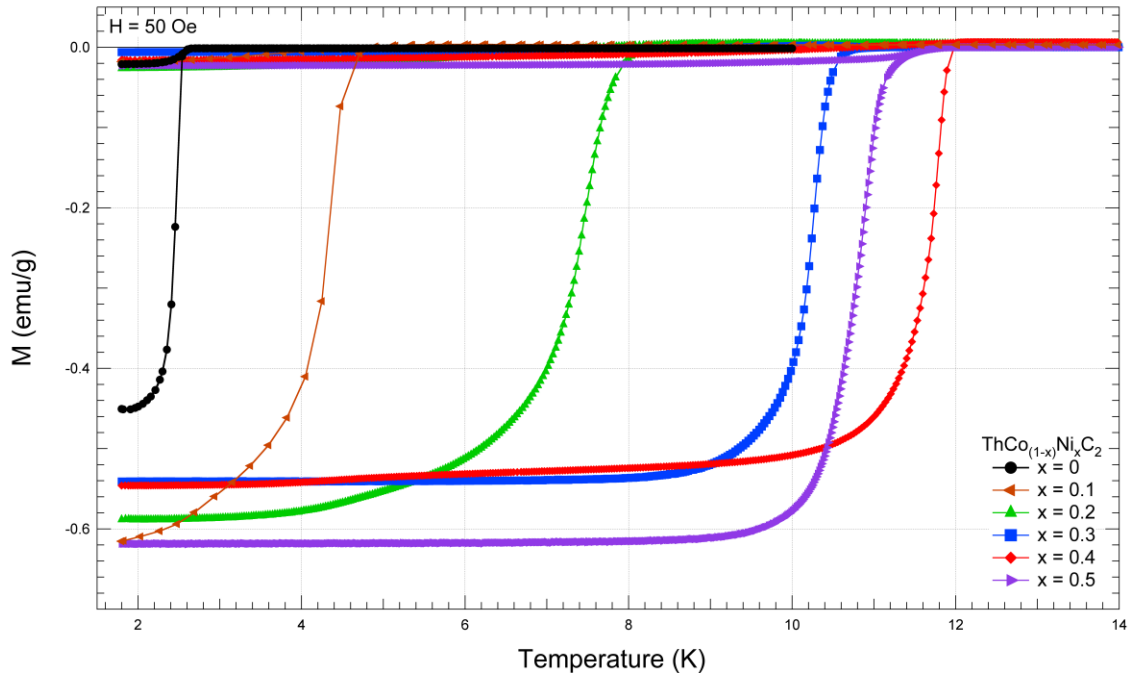


FIG. 2. Magnetization measurements for samples $\text{ThCo}_{1-x}\text{Ni}_x\text{C}_2$ using ZFC and FC temperature sweeps with an applied magnetic field of $H = 50$ Oe.

The confirmation of the superconducting transitions by resistivity measurements of the $\text{ThCo}_{1-x}\text{Ni}_x\text{C}_2$ samples are shown in Fig. 3. The resistivity transition temperatures are in good agreement with the magnetization measurements. The critical temperature is again maximized for the sample $x=0.4$ with $T_c=12.1\text{K}$ (transition midpoint). The residual resistivity values for the samples range from $30 \text{ m}\Omega \cdot \text{cm}$ to $90 \text{ m}\Omega \cdot \text{cm}$, much higher than

the $0.37 \text{ m}\Omega \cdot \text{cm}$ for the parent compound ThCoC_2 . Not surprisingly, the residual resistivity ratio (RRR) is significantly smaller, ranging from 5.5 to 2.1 for the Ni substituted samples $\text{ThCo}_{1-x}\text{Ni}_x\text{C}_2$, compared to the huge 218 for ThCoC_2 . The decrease in the RRR is expected for the quasi-ternary system $\text{ThCo}_{1-x}\text{Ni}_x\text{C}_2$ as the addition of an extra element complicates the material phase diagram, increasing the likelihood to have inhomogeneities and disorder effects in the sample and thus increasing the amount of scattering centers that raise the residual resistivity.

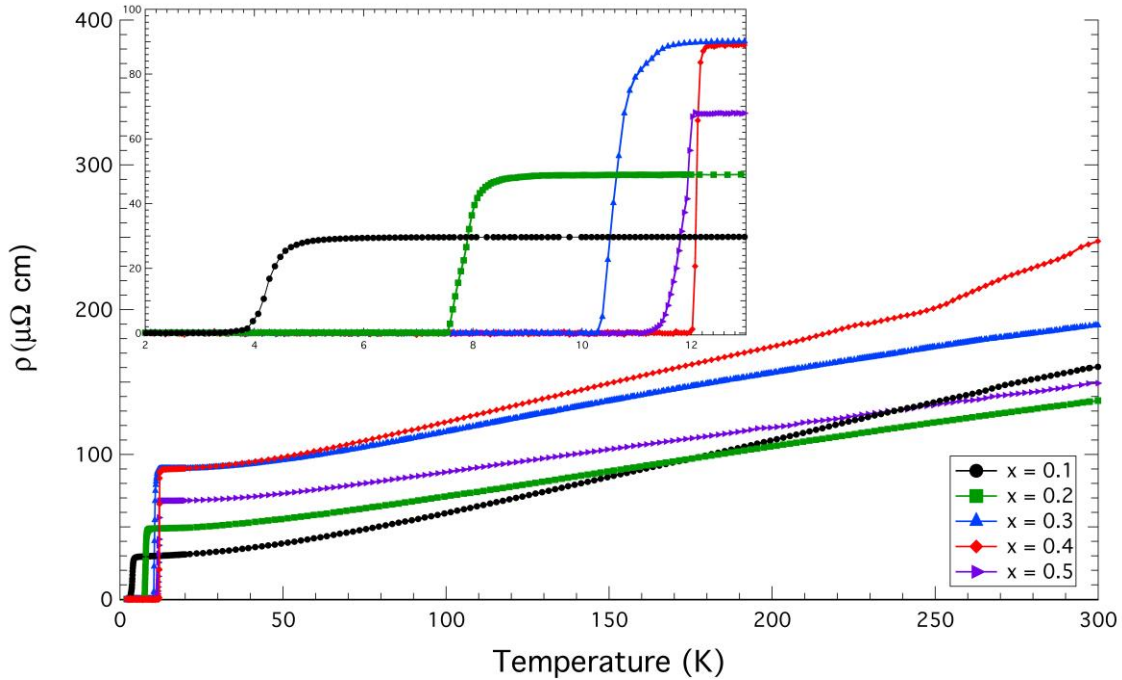


FIG. 3. Temperature dependent resistivity measurement for samples $\text{ThCo}_{1-x}\text{Ni}_x\text{C}_2$ without applied magnetic field. Inset shows the superconducting transitions at low temperature.

It is clear from the resistivity and magnetization measurements that the Ni substitution increases the superconducting transition temperature dramatically. However, heat capacity measurements are required to confirm the transition from the Ni substitution is a bulk transition and not a filamentary or surface effect. The specific heat measurements with and without applied magnetic field display discontinuities that confirm bulk superconductivity in the $\text{ThCo}_{1-x}\text{Ni}_x\text{C}_2$ samples. Figure 4 displays the electronic contribution C_e to the specific heat, obtained by subtracting off the lattice contribution to the specific heat using a Debye model fit to the normal state specific heat data.

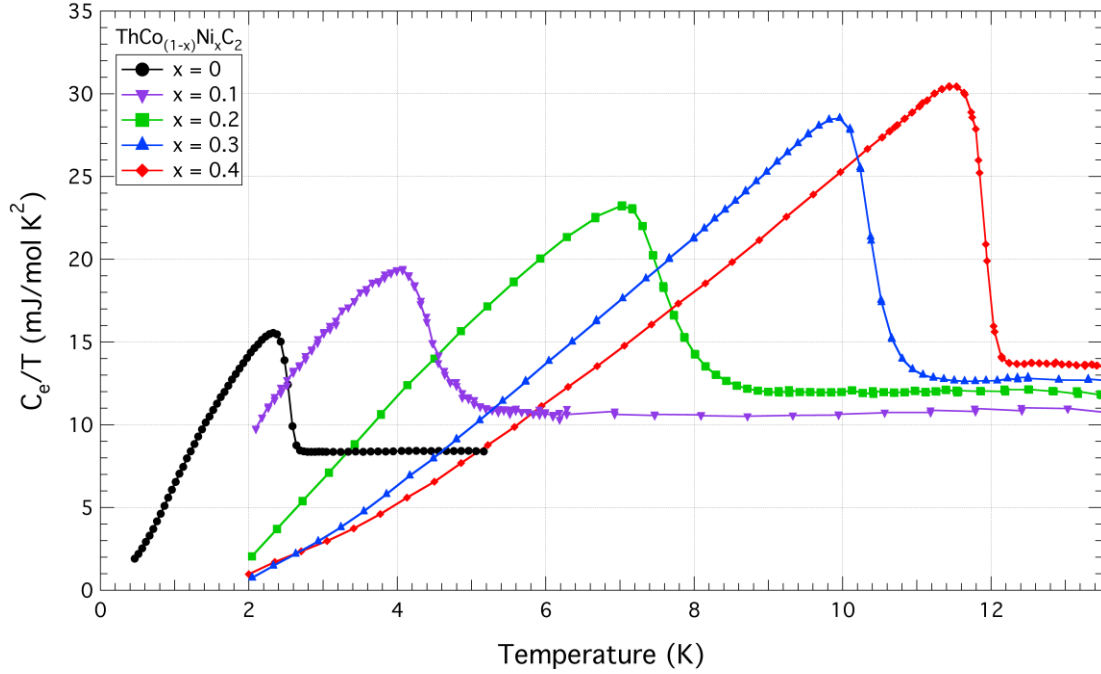


FIG. 4. The electronic specific heat divided by temperature (C_e/T) plotted against temperature for the samples $\text{ThCo}_{1-x}\text{Ni}_x\text{C}_2$.

In good agreement with the previous characteristic measurements, the critical temperature is maximized at $T_c=11.9\text{K}$ in the sample with Ni concentration of $x=0.4$. The Sommerfeld coefficients γ also increase from $8.38\text{ mJ}/(\text{mol K}^2)$ in the pure compound to $13.7\text{ mJ}/(\text{mol K}^2)$ in the $x=0.4$ sample, which is shown in Table I. For noninteracting particles the Sommerfeld coefficient is proportional to the electronic density of states at the Fermi level $D(E_F)$. However, in real materials the additional electron-phonon interaction increases the measured electronic specific heat coefficient by an enhancement factor $(1+\lambda_{e-ph})$, where λ_{e-ph} is the dimensionless electron-phonon coupling constant. The measured Sommerfeld coefficient is thus proportional to the bare band-structure density of states $N(0)$ by the relation:

$$g = \left(\frac{\rho^2 k_B^2}{3}\right) N(0) (1 + \lambda_{e-ph}) \quad (1)$$

In superconducting materials, the electron-phonon coupling constant can be calculated using the measured Debye Temperature Θ_D and critical temperature T_c by the McMillan formula⁴⁰:

$$l_{e-ph} = \frac{1.04 + m^* \ln(q_D/1.45T_c)}{(1 - 0.62m^*) \ln(q_D/1.45T_c) - 1.04} \quad (1)$$

where μ^* is the repulsive screened Coulomb parameter, which is typically estimated to be $\mu^* = 0.13$ for many intermetallic superconductors. Using these two relations we can calculate both the electron-phonon coupling constant λ_{e-ph} and the electronic density of states $N(0)$ from the specific heat measurements, which are displayed in Table I. The Ni substitution increases both the electron-phonon coupling and the electronic density of states significantly, with the increase in the $N(0)$ being the dominant effect. This result is consistent with the BCS theory, where an increasing density of states or electron-phonon coupling will raise the critical temperature. In fact, it appears that the superconducting critical temperature T_c strongly favors an increased electron count in this NCS system, where Ni substitution effectively dopes electrons into ThCoC_2 . This behavior was also observed in isoelectronic LaNiC_2 , where an increase in electron count by Th substitution into $\text{La}_{1-x}\text{Th}_x\text{NiC}_2$ strongly enhanced the critical temperature up to $T_c = 7.9\text{K}$ for $x = 0.5$.^{41,42} The small suppression effect by chemical pressure with Th substitution is overcome by the strong enhancement to the critical temperature due to the increased electron count in the band structure. Here the Ni substitution into $\text{ThCo}_{1-x}\text{Ni}_x\text{C}_2$ contributes the dual enhancement due to an increased electron count and electron-phonon coupling, and thus has a larger critical temperature compared to the $\text{La}_{1-x}\text{Th}_x\text{NiC}_2$ system.

Table I. Superconducting and normal state properties from the heat capacity measurements for $\text{ThCo}_{1-x}\text{Ni}_x\text{C}_2$.

x	T_c (K)	Y mJ mol ⁻¹ K ⁻¹	Θ_D (K)	λ_{e-ph}	ΔC_e/YT_c	N(0) (eV f.u.) ⁻¹
0	2.55	8.38	449	0.493	0.86	2.38
0.1	4.4	10.7	454	0.553	0.83	2.92
0.2	7.6	11.7	542	0.610	0.95	3.08
0.3	10.4	12.5	520	0.677	1.25	3.16
0.4	11.9	13.7	584	0.681	1.23	3.46

Also of particular interest is the evolution of the relative size of the specific heat jump DC_e/gT_c , which is expected to be 1.43 in the weak-coupling BCS limit. The pure ThCoC_2 compound is significantly smaller than the predicted value at 0.86, which could arise from a multi-gap or anisotropic gap structure. With Ni substitution, the specific heat

jump increases significantly to 1.23 for the $x=0.4$ sample. This suggests that not only is the critical temperature increasing dramatically with Ni substitution on the Co site, but the characteristic of the superconducting state is being tuned as well towards a more fully gapped order parameter. This is perhaps an evolution from a strong multiband or mixed-parity pairing state that is allowed in NCS superconductors and towards the more conventional spin-singlet state. Future band structure calculations of ThCoC_2 are needed to illuminate both the evolution of the density of states and the possible tuning of the ASOC with Ni substitution on the Co site.

The phase diagram of the superconducting critical temperature T_c with respect to Ni substitution is displayed in Fig. 5. The critical temperature T_c for the resistivity and heat capacity measurements are the transitions midpoints, and the magnetization measurements are the transition onset. The three characteristic measurements are in good agreement with each other up to concentration $x=0.4$. At Ni concentration $x=0.5$ there starts to be a divergence between the measurements as the solubility limit for Ni substitution has been reached that results in a reduced superconducting volume fraction, and at higher concentration we see a breakdown of a bulk single phase.

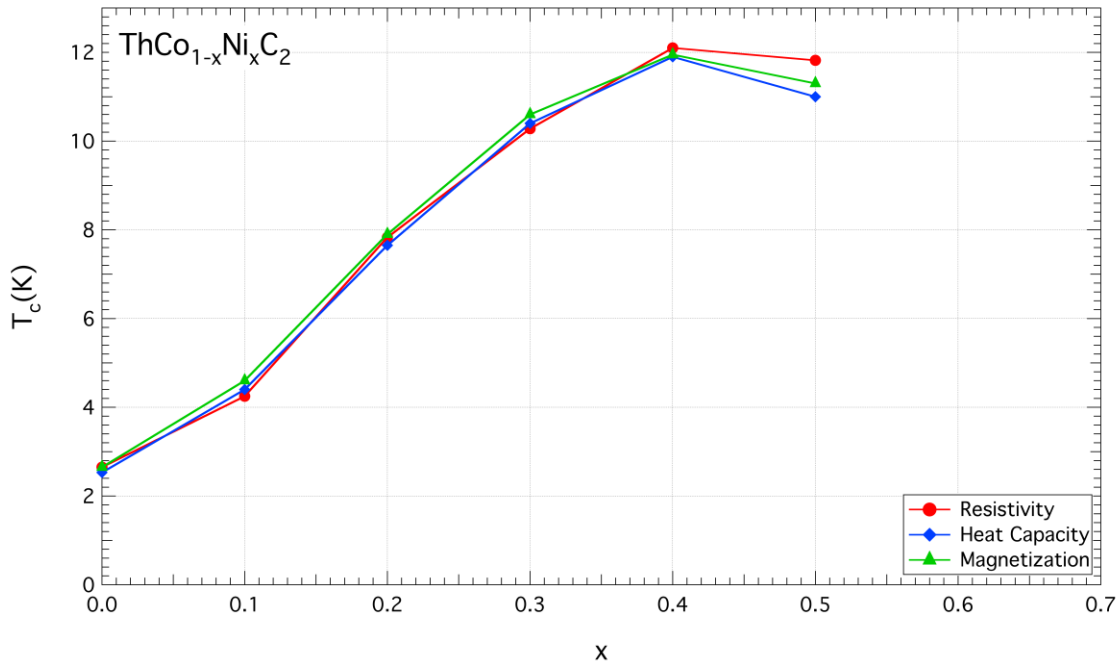


FIG. 5. The superconducting critical temperature T_c vs. Ni concentration x from the resistivity, magnetization, and heat capacity measurements.

Figure 6 shows the upper critical field H_{c2} phase diagram with respect to temperature, where the midpoint of the resistivity transitions are used. From this figure it is clear that the Ni doping systematically increases $H_{c2}(T)$ from the pure compound to the optimally doped sample with $x=0.4$, which is estimated to reach 13T. The evolution of the $H_{c2}(T)$ behavior with the Ni doping is remarkable and clearly shows a change to a more linear behavior. A pronounced positive curvature governs the behavior of pure ThCoC_2 , whereas the doped samples have a small positive curvature near T_c that then transitions to a more linear dependence. This latter behavior is similar to what is observed in some multiband and noncentrosymmetric superconductors such as Y_2C_3 , CeRhSi_3 , $\text{Li}_2(\text{Pt,Pd})_3\text{B}$, and also LaNiC_2 . For a clear comparison, the inset shows the normalized upper critical field $H_{c2}/[T_c(dH_{c2}/dT)_{T_c}]$ versus reduced temperature T/T_c using the Werthamer-Helfand-Hohenberg (WHH) model. The extraordinary large positive curvature in pure ThCoC_2 is clearly apparent, which is then suppressed in $x=0.4$ towards a more linear yet enhanced H_{c2} compared to the WHH model for conventional superconductors. This enhancement of H_{c2} can arise in multiband superconductors from the contribution of the smaller gap at low temperature. It is possible for NCS superconductors to display multiband characteristics when the ASOC has a moderate effect on the pairing state, giving the spin singlet and triplet channels comparable contributions.

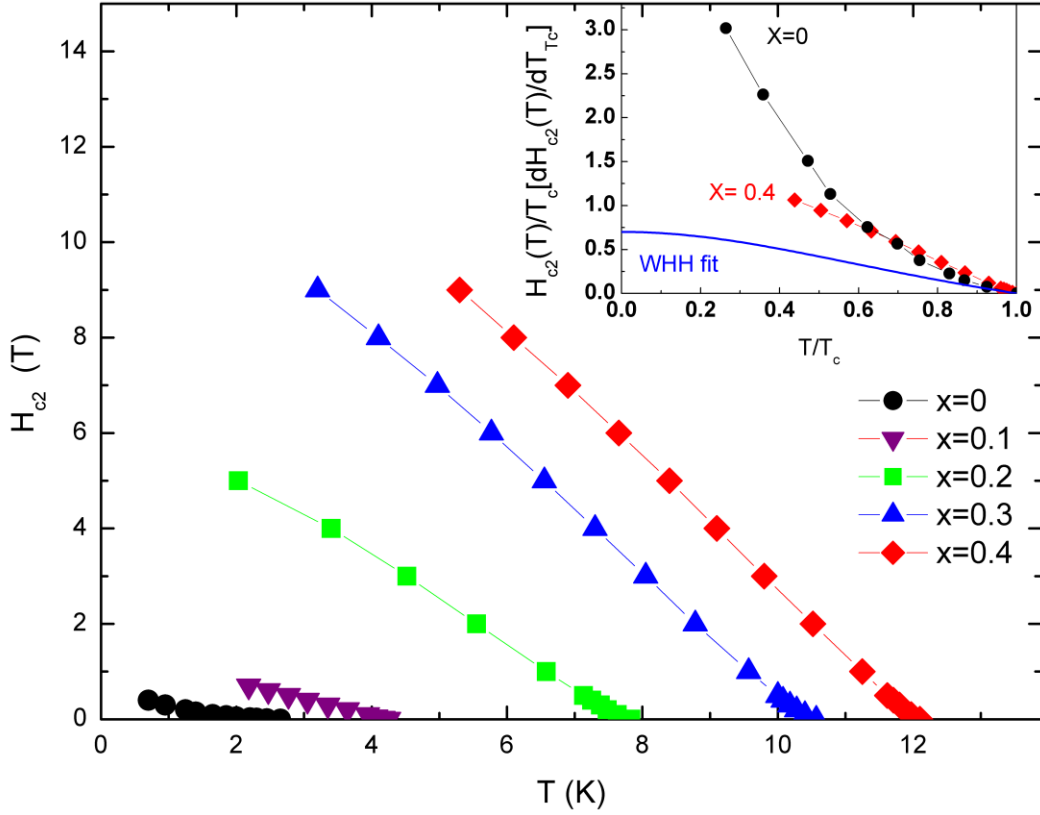


FIG. 6. The superconducting phase diagram of the upper critical field H_{c2} vs. temperature from the resistivity measurements. The inset shows the normalized H_{c2} plotted against the reduced temperature T/T_c for the $x=0$ and $x=0.4$ samples, with the solid blue curve representing the conventional WHH behavior.

Figure 7 shows the magnetic field dependence of the normalized residual Sommerfeld coefficients $\gamma_0(H)/\gamma_n$ plotted against the reduced applied magnetic field $H/H_{c2}(0)$. The residual Sommerfeld coefficient $\gamma_0(H)$ in the superconducting state gives important information about the low-energy excitations which exist near the Abrikosov vortex line. In fully gapped superconductors, the low-energy excitations are confined to the vortex cores in the normal state with the radius proportional to the penetration depth ξ . In this case, the specific heat is proportional to the vortex density and is a linear function⁴³ of the magnetic field, $\gamma_0(H) \propto H$. In other superconductors with nodes in the energy gap,

the density of states is concentrated in the vicinity of the gap nodes, because the low energy excitations are outside the vortex core and therefore is expected^{44,45} to show square root dependence $g_0(H) \propto H^{1/2}$. The values of $H_{c2}(0)$ are extrapolated from the specific heat data for ThCoC₂ and for the $H_{c2}(T)$ functions for the Ni doped compounds. The values were obtained from the data at $0.15T_c$, after subtracting the small residue in zero magnetic field. From the figure, the experimental results for the pure ThCoC₂ compound presents a fast increase of $\gamma_0(H)$ at low fields and then a saturation at higher fields. This characteristic clearly deviates from both the linear fully gap behavior and the nodal square root behavior, which is represented by the solid blue curve in Figure 7. The field dependence of $\gamma_0(H)$ in ThCoC₂ is similar to what is observed in LaNiC₂ and is suggestive of a possible multigap scenario.³⁵ A systematic transition from this anomalous behavior towards a fully gapped BCS like linear dependence can be seen for the Ni doped samples from $x=0$ to $x=0.4$. It is remarkable how the Ni doping induces a dramatic change, which results in the $x=0.4$ sample being nearly linear. Such a dramatic change could be related to a shift in the band structure or a reduction in the ASOC that is responsible for the triplet pairing contribution to the parameter order. The best example of ASOC tuning is in Li₂(Pd,Pt)₃B, where increasing Pt substitution increased the ASOC and strengthened the spin-triplet component, leading to a nodal gap superconductivity in Li₂Pt₃B.^{17,18} It should be noted however, that the characteristic field dependence of $\gamma_0(H)$ is not definitive evidence to determine the symmetry of the superconducting gap. Although this characteristic was considered a common signature on d-band superconductors and heavy fermions,⁴⁶⁻⁴⁸ non-linear behaviors have also been reported in some conventional BCS superconductors, with examples such as V₃Si, NbSe₂, and CeRu₂.⁴⁹⁻⁵² Therefore, the behavior observed here could

be a transition from the clean limit in ThCoC_2 to the dirty limit with Ni substitution in $\text{ThCo}_{1-x}\text{Ni}_x\text{C}_2$. In either case, the evolution of the superconductivity in $\text{ThCo}_{1-x}\text{Ni}_x\text{C}_2$ is intriguing and warrants additional detailed studies of these phenomena to elucidate the superconducting gap structure, and whether or not a multiband scenario is adequate to explain these results.

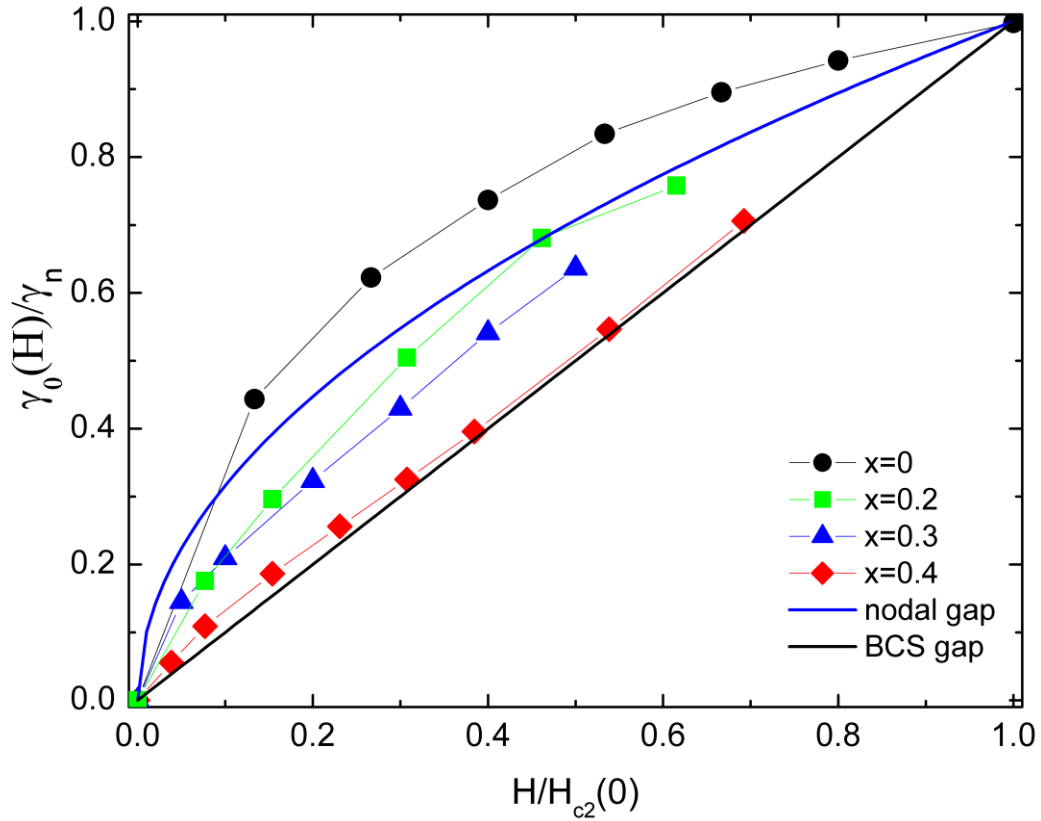


FIG. 7. Magnetic field dependence of the normalized residual Sommerfeld coefficient $\gamma_0(H)/\gamma_n$ as a function of the normalized applied field $H/H_{c2}(0)$. The solid blue curve represents the square root dependence expected for a nodal gap, and conventional BCS behavior is expected to show linear dependence.

IV. CONCLUSIONS

In summary, we have studied the effects of systematic substitution of Ni into the noncentrosymmetric superconducting system $\text{ThCo}_{1-x}\text{Ni}_x\text{C}_2$ by magnetization, resistivity,

and heat capacity measurements. The addition of Ni increases the electron count that dramatically favors the superconducting state. The critical temperature is significantly increased up to $T_c=12.1\text{K}$ ($4.5T_c$ of ThCoC_2) and an estimated upper critical field of $H_{c2}(0)=13\text{T}$, which are both maximized with Ni concentration of $x=0.4$. Additionally, the unconventional superconducting behavior observed in ThCoC_2 (reduced jump and nonexponential temperature dependence in C_e , extreme positive curvature in H_{c2} , and the magnetic field dependence of the residual Sommerfeld coefficients) appears to be suppressed or tuned towards a more conventional full gapped superconducting state. The interesting nature of the superconductivity in ThCoC_2 and the large effect by Ni substitution presents several possibilities for future investigations. The role of ASOC in NCS superconductors and the large influence of Ni substitution on the density of states creates a large need for band structure calculations on ThCoC_2 . Additional low temperature measurements, such as magnetic penetration depth, should help illuminate the nature of the superconducting gap structure in ThCoC_2 .

ACKNOWLEDGMENTS

This work was generously supported by grants from the AFOSR-MURI and FAPESP (2014/25241-3).

REFERENCES

- ¹ J. Bardeen, L. N. Cooper, and J. R. Schrieffer, Phys. Rev. **108**, 1175 (1957).
- ² P. W. Anderson, J. Phys. Chem. Solids **11**, 26 (1959).
- ³ P. W. Anderson, Phys. Rev. B **30**, 4000 (1984).
- ⁴ L. P. Gor'kov and E. I. Rashba, Phys. Rev. Lett. **87**, 037004 (2001).
- ⁵ K. V. Samokhin, E. S. Zijlstra, and S. K. Bose, Phys. Rev. B **69**, 094514 (2004).
- ⁶ P. A. Frigeri, D. F. Agterberg, A. Koga, and M. Sigrist, Phys. Rev. Lett. **92**, 097001 (2004).
- ⁷ S. Fujimoto, J. Phys. Soc. Jpn. **76**, 051008 (2007).

- ⁸ S.K. Yip, Phys. Rev. B **65**, 144508 (2002).
- ⁹ E. Bauer and M. Sigrist, *Non-Centrosymmetric Superconductors: Introduction and Overview* (Springer Science and Business Media, Berlin, 2012), Vol. 847.
- ¹⁰ M. Smidman, M.B. Salamon, H.Q. Yuan, and D.F. Agterberg, Rep. Prog. Phys. **80**, 036501 (2017).
- ¹¹ E. Bauer, G. Hilscher, H. Michor, C. Paul, E. W. Scheidt, A. Griбанov, Y. Seropegin, H. Noel, M. Sigrist, and P. Rogl, Phys. Rev. Lett. **92**, 027003 (2004).
- ¹² T. Akazawa, H. Hidaka, H. Kotegawa, T. C. Kobayashi, T. Fujiwara, E. Yamamoto, Y. Haga, R. Settai, and Y. Onuki, J. Phys. Soc. Jpn. **73**, 3129 (2004).
- ¹³ N. Kimura, K. Ito, H. Aoki, S. Uji, and T. Terashima, Phys. Rev. Lett. **98**, 197001 (2007).
- ¹⁴ R. Settai, Y. Miyauchi, T. Takeuchi, F. Levy, I. Sheikin, and Y. Onuki, J. Phys. Soc. Jpn. **77**, 073705 (2008).
- ¹⁵ K. Togano, P. Badica, Y. Nakamori, S. Orimo, H. Takeya, and K. Hirata, Phys. Rev. Lett. **93**, 247004 (2004).
- ¹⁶ P. Badica, T. Kondo, and K. Togano, J. Phys. Soc. Jpn. **74**, 1014 (2005).
- ¹⁷ M. Nishiyama, Y. Inada, and G.Q. Zheng, Phys. Rev. Lett. **98**, 047002 (2007).
- ¹⁸ H. Q. Yuan, D. F. Agterberg, N. Hayashi, P. Badica, D. Vandervelde, K. Togano, M. Sigrist, and M. B. Salamon, Phys. Rev. Lett. **97**, 017006 (2006).
- ¹⁹ K.W. Lee and W. E. Pickett, Phys. Rev. B **72**, 174505 (2005).
- ²⁰ J. Chen, M. B. Salamon, S. Akutagawa, J. Akimitsu, J. Singleton, J. L. Zhang, L. Jiao, and H. Q. Yuan, Phys. Rev. B **83**, 144529 (2011).
- ²¹ S. Kuroiwa, Y. Saura, J. Akimitsu, M. Hiraishi, M. Miyazaki, K.H. Satoh, S. Takeshita, and R. Kadono, Phys. Rev. Lett. **100**, 097002 (2008).
- ²² T. Klimczuk, F. Ronning, V. Sidorov, R. J. Cava, and J. D. Thompson, Phys. Rev. Lett. **99**, 257004 (2007).
- ²³ Y. Qi, J. Guo, H. Lei, Z. Xiao, T. Kamiya, and H. Hosono, Phys. Rev. B **89**, 024517 (2014).

- ²⁴ L. Fang, H. Yang, X. Zhu, G. Mu, Z. S. Wang, L. Shan, C. Ren, and H.-Hu Wen, *Phys. Rev. B* **79**, 144509 (2009).
- ²⁵ E. Bauer, G. Rogl, X.-Q. Chen, R. T. Khan, H. Michor, G. Hilscher, E. Royanian, K. Kumagai, D. Z. Li, Y. Y. Li, R. Podloucky, and P. Rogl, *Phys. Rev. B* **82**, 064511 (2010).
- ²⁶ N. Kase and J. Akimitsu, *J. Phys. Soc. Jpn.* **78**, 044710 (2009).
- ²⁷ W.H. Lee, H.K. Zeng, Y.D. Yao, and Y.Y. Chen, *Physica C* **266**, 138 (1996).
- ²⁸ V. K. Pecharsky, L. L. Miller, and K. A. Gschneidner, Jr., *Phys. Rev. B* **58**, 497 (1998).
- ²⁹ Y. Iwamoto, Y. Iwasaki, K. Ueda, and T. Kohara, *Phys. Lett. A* **250**, 439 (1998).
- ³⁰ O.I. Bodak and E.P. Marusin, *Dopov. Akad. Nauk Ukr. SSR Ser. A* **12**, 1048 (1979).
- ³¹ W. Schafer, W. Kockelmann, G. Will, J.K. Yakinthos, and P.A. Kotsanidis, *J. Alloys Compounds* **250**, 565 (1997).
- ³² S. Shimomura, C. Hayashi, N. Hanasaki, K. Ohnuma, Y. Kobayashi, H. Nakao, M. Mizumaki, and H. Onodera, *Phys. Rev. B* **93**, 165108 (2016).
- ³³ A. D. Hillier, J. Quintanilla, and R. Cywinski, *Phys. Rev. Lett.* **102**, 117007 (2009).
- ³⁴ I. Bonalde, R.L. Ribeiro, K.J. Syu, H.H. Sung, and W.H. Lee, *New J. Phys.* **13**, 123022 (2011).
- ³⁵ J. Chen, L. Jiao, J.L. Zhang, Y. Chen, L. Yang, M. Nicklas, F. Steglich, and H.Q. Yuan, *New J. Phys.* **15**, 053005 (2013).
- ³⁶ T. Grant, A.J.S. Machado, D.J. Kim, and Z. Fisk, *Supercond. Sci. Technol.* **27**, 035004 (2014).
- ³⁷ A. Subedi and D.J. Singh, *Phys. Rev. B* **80**, 092506 (2009).
- ³⁸ H. H. Sung, S.Y. Chou, K.J. Syu, and W.H. Lee, *J. Phys. Condens. Matter* **20**, 165207 (2008).
- ³⁹ T.F. Liao, H.H. Sung, K.J. Syu, and W.H. Lee, *Solid State Commun.* **149**, 448 (2009).
- ⁴⁰ W.L. McMillan, *Phys. Rev.* **167**, 331 (1968).
- ⁴¹ W.H. Lee and H.K. Zeng, *Solid State Commun.* **101**, 323 (1997).
- ⁴² W.H. Lee, H.K. Zeng, Y.Y. Chen, Y.D. Yao, and J.C. Ho, *Solid State Commun.* **102**, 433 (1997).

- ⁴³ C. Caroli, P.G. de Gennes and J. Matricon, *Phys. Lett.* **9**, 307 (1964).
- ⁴⁴ G.E. Volovik, *Pisma Zh. Eksp. Teor. Fiz.* **58**, 457 (1993).
- ⁴⁵ G.E. Volovik, *JETP Lett.* **58**, 469 (1993).
- ⁴⁶ D.A. Wright, J. Emerson, B. Woodfield, J. Gordon, R. Fisher, and N. Phillips, *Phys. Rev. Lett.* **82**, 1550 (1999).
- ⁴⁷ H.D. Yang and J.Y. Lin, *J. Phys. Chem. Solids* **62**, 1861 (2001).
- ⁴⁸ H.P. van der Meulen, Z. Tarnawski, A. de Visser, J. Franse, J. Perenboom, D. Althof, and H. van Kempen, *Phys. Rev. B* **41**, 9352 (1990).
- ⁴⁹ D. Sanchez, A. Junod, J. Muller, H. Berger, and F. Levy, *Physica (Amsterdam)* **204B**, 167 (1995).
- ⁵⁰ J.E. Sonier, M.F. Hundley, J.D. Thompson, and J.W. Brill, *Phys. Rev. Lett.* **82**, 4914 (1999).
- ⁵¹ A.P. Ramirez, *Phys. Lett. A* **211**, 59 (1996).
- ⁵² M. Hedo, Y. Inada, E. Yamamoto, Y. Haga, Y. Onuki, Y. Aoki, T.D. Matsuda, H. Sato, and S. Takahashi, *J. Phys. Soc. Jpn.* **67**, 272 (1998).